ELSEVIER

Sensors and Actuators A 71 (1998) 223–229

SENSORS AND ACTUATORS A PHYSICAL

Design and implementation of PCB-type capacitance displacement sensor collocated with magnetic bearings

Dongwon Shin [a,*], Jongwon Kim [b]

[a] School of Mechanical Engineering, Kumoh National University of Technology, 188 Shinpyung-dong Kumi, Kyungbuk 730-701, South Korea
[b] Department of Mechanical Design and Production Engineering, Seoul National University, San 56-1 Shinlim-dong, Kwanak-ku, Seoul 151-742, South Korea

Received 29 May 1998; accepted 4 June 1998

Abstract

This paper presents the design of a printed circuit board (PCB)-type capacitance displacement sensor with the capability of being collocated with a magnetic bearing. The capacitance sensor is less influenced by a magnetic field environment than other sensors, and the desired capacitor pattern that can be fitted to the magnetic bearing is easily manufactured using PCB technology, so that the developed sensor can be collocated with a magnetic bearing. The sensor signal-processing unit drives the sensor by means of a switching method. Performance evaluation of the sensor has been carried out for both static and dynamic characteristics. Finally, the experimental behaviors on the output of the sensor are described for application to the control of the magnetic bearing system. © 1998 Elsevier Science S.A. All rights reserved.

Keywords: Capacitance sensor; PCB; Collocation; Sensitivity; Bandwidth; Magnetic bearing

1. Introduction

Capacitance sensors have long been used in applications for distance, fill level and pressure sensors. The capacitance sensor has advantages in that it is simple in construction and is highly sensitive. However, as a transducer it costs more than inductive (eddy current) or resistive-type transducers, and its associated electronics are somewhat more complex than other common types of transducers.

The main ideas about this research are based on three points. The first point is that the developed sensor is made of a small piece of a printed circuit board (PCB) so that it will be cost-effective, light in weight and compact enough to be integrated into a magnetic bearing system. The second point is that the sensor is not a probe-type but rather a plate-type so that the large area can reduce the effect of roughness in the measured object. The final point is to collocate the sensor with a magnetic bearing to overcome the problem of non-collocation.

Bonse et al. [1] used PCB technology to manufacture a capacitance sensor to measure two-dimensional motions. Measurement of position by switching the charge is one of many capacitance-sensing methods for measuring a gap. This has been well demonstrated by Chapman [2]. He installed a circular brass sensor plate at the end of the spindle nose of a milling machine to measure the motion of the rotor. The voltage across the capacitor electrode and the rotor is sampled at the end of a charging time, thus, ultimately measuring the rotational motion accuracy about the spindle axis. The research approach used in this paper is based on Chapman's method. However, this research has been enhanced by the recognition that the sensor size can be significantly reduced by adopting a PCB manufacturing technology instead of a machined brass layer. In addition, a feedback circuit that maintains constant current to the capacitor during the charging time is attached to a sensor drive unit in order to improve the sensitivity of the sensor.

The displacement sensor most frequently used in magnetic bearing control is the eddy current sensor since it has high resolution and wide bandwidth [3]. This type of sensor is very easily influenced by the magnetic field generated in magnetic bearing coils and so should be installed outside the coils [4]. This causes non-collocation between the gap-measuring sensor and the magnetic bearing coils. Moreover, the non-collocated magnetic bearing can generate unstable motions to a flexible shaft [5,6]. The capacitance sensor is not intrinsically affected by the magnetic field. However, most commercial capacitance sensors are relatively expensive and are not sufficiently compact for collocating in a

* Corresponding author. Tel.: +82-546-467-4380; Fax: +82-546-467-4200.

0924-4247/98/$ - see front matter © 1998 Elsevier Science S.A. All rights reserved.
PII S0924-4247(98)00192-7

magnetic bearing. Salazar et al. [7] used a plate-type capacitance sensor in a magnetic bearing system, but this sensor is not collocated with the magnetic actuator. Due to the fact that our developed sensor is capacitive and easily fitted to the magnetic bearing using PCB manufacturing technology, the sensor can be collocated with the magnetic bearing coils.

Experimental results show the sensitivity and bandwidth performance of two sensors of different size. Finally, the experimental results related to the control of the magnetic bearing system demonstrate the practicability of the collocated capacitance sensor.

2. Design of the capacitance sensor

Fig. 1 shows the sensor built in the magnetic bearing as well as the shape of the designed capacitance sensor plate. The arrangement with four sensors located between the poles of the magnetic bearing is designed to eliminate the non-collocation problem of the sensor. A difference in output between opposite sensors represents the displacement of a rotor on one axis. The base material of the sensor plate is epoxy resin FR4, and it is coated with a copper layer 0.1 mm thick. The copper layer is then cut to the desired pattern through an etching process, which is identical technology to that used in PCB manufacture. The copper layer pattern is composed of a sensor element and a guard area, as seen in Fig. 1. The sensor element is the main capacitive element that measures the gap displacement. The guard area surrounding the sensor element prevents leakage of sensor element electric charge and protects the sensor element signals from interference external to the sensor plate.

Fig. 2 shows the detailed geometric dimensions of the two differently sized sensor plates that were developed. The dimensions in parenthesis refer to those of the larger size plate. The plate sizes are 48.5×8.0 mm (sensor #1) and 68.5×8.0 mm (sensor #2), each 1.6 mm thick, which are maximized sizes to achieve more sensitivity, considering the space between magnetic bearing poles. The two holes on the left side are used for wiring connections. When the gap between the object and the sensor is 0.2 mm, the measured capacitances of sensor #1 and sensor #2 are 9 and 17 pF, respectively. Finally, the surface of the sensor plate is coated with solder mask in order to create an insulated protection layer.

The sensor signal-processing unit as shown in the schematic diagram of Fig. 3 has four sensor channels, each of which can measure the displacement signal individually. The final gap displacements on the x-axis (y-axis) are measured by subtracting the signals from one gap sensor from those of the opposing sensor. This subtracting process has the effect of doubling the sensitivity and canceling any common-mode noise error.

The signal-processing unit consists of two parts: (1) four capacitance-to-voltage converters (C/Vs), four sample-and-hold circuits (S/Hs) and four offset-gain adjustment circuits

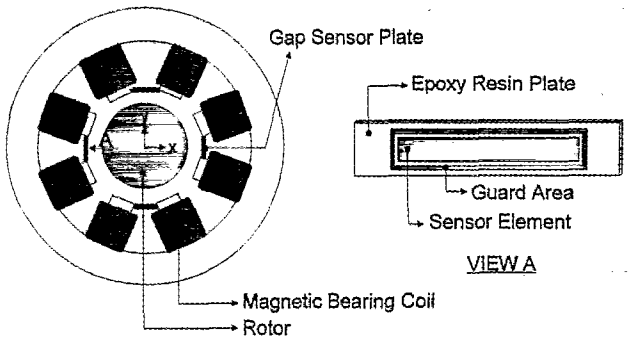

Fig. 1. Collocated sensor built in the magnetic bearing and the shape of the sensor plate.

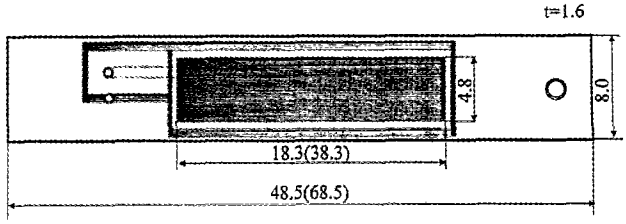

Fig. 2. Detailed geometric dimensions of the capacitance sensor plate (unit: mm).

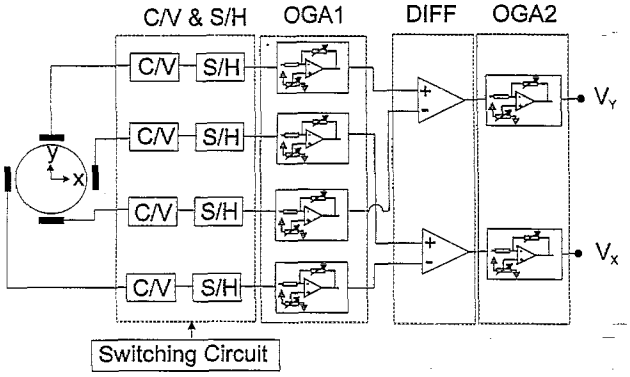

Fig. 3. Schematic diagram of the signal-processing unit.

(OGA1s); and (2) two differential circuits (DIFFs) and two offset-gain adjustment circuits (OGA2s).

The measure of the capacitance of the sensor according to gap displacement variation is measured as a voltage through the C/V. This measure is sampled and held though the S/H. The function of the OGA1 is to adjust the offset and the gain of each channel. The differential signal of the DIFF is finally adjusted through the OGA2. The actual offset adjustment is carried out by OGA2 rather than by OGA1.

Fig. 4(a) shows the signal flow chart of the C/V and the S/H where charging, sampling and holding, and discharging of the sensor element take place. Fig. 4(b) illustrates the detailed circuits of the C/V and the S/H in the signal-processing unit. The function of the C/V is to charge the sensor element with a constant current during a fixed charging time interval T_c when the driving signal V_{CD} is low, and similarly, to discharge the sensor during a fixed discharging time interval T_d when V_{CD} is high. If switch #1 (SW1) is open as V_{CD} drops to a low driving signal, the charging current i_s flows to

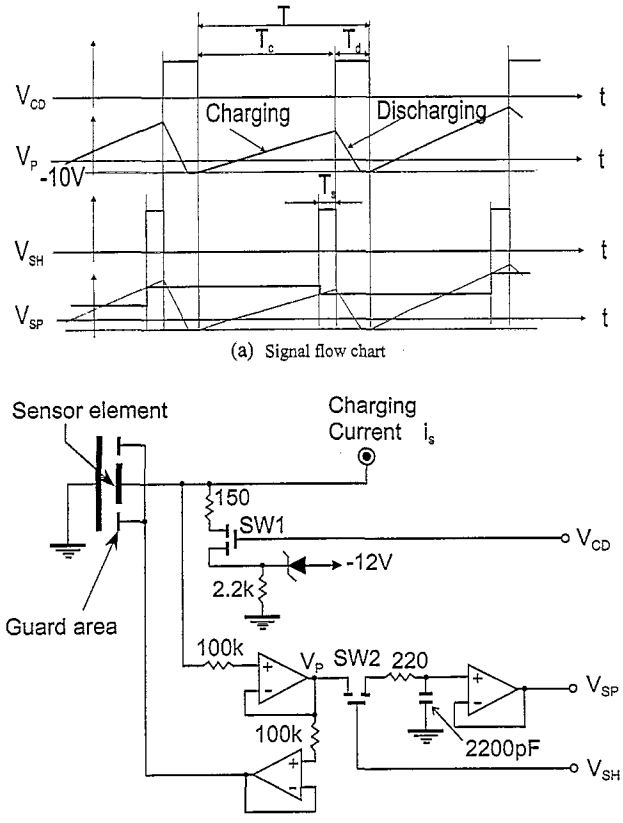

Fig. 4. Signal flow chart and detailed circuits of the C/V and S/H of the signal-processing unit.

the sensor element that is to be charged, so that V_p is increased from -10 V to a voltage dependent on the gap displacement x. When V_{CD} rises to a high driving signal, SW1 is closed and the sensor element is discharged, so that V_p falls quickly to -10 V. The voltage of the guard area changes synchronously with the sensor element by means of voltage followers. In charging the sensor element, a constant current circuit with a feedback loop was adopted instead of the constant voltage circuit used by Chapman. This was because it is difficult for a constant voltage circuit to supply a constant current during the charging time without deteriorating the linearity of V_p with respect to time.

The function of the S/H is to sample and hold the charged voltage V_p of the sensor element as the sample and hold driving signal V_{SH} turns switch #2 (SW2) on and off in the circuit. The maximum value of the charged voltage V_p of the sensor element can be sampled towards the end of charging, creating the output signal V_{sp}. As soon as V_p is sampled, the C/V discharges the remaining electric charges present in the sensor element. The operations of charging, sampling and holding, and discharging are executed repeatedly during a cycle time T within the circuit of the C/V and the S/H.

The output voltage V_{sp} is proportional to the gap displacement, as seen from the equations generally used for a parallel plate capacitor: $C=\varepsilon_0\varepsilon_r A/d$ and $V_{sp}=Q/C$, where Q is the electric charge in the capacitor, C the value of the capacitance, ε_r the relative dielectric permittivity of the surrounding medium, ε_0 the dielectric permittivity of vacuum, and A the area of the capacitor. The typical values of cycle time T, discharging time T_d, and sampling time T_s are 57–65 μs, 15 μs and 440 ns, respectively, in this research.

3. Experimental evaluation on static performance of the developed sensor

The static characteristics of the sensor, subject to variation of the charging current, cycle time and gap displacement, have been evaluated experimentally as performance measures of the sensor.

An experimental setup was implemented whereby a sensor system is attached to the moving part of a micrometer that retains the positioning accuracy of 10 μm resolution. The sensor plates can be positioned accurately from the rotor in the radial direction by moving the micrometer. The output signal V_x of the signal-processing unit is measured for each position of the sensor plate. The curve 1 of Fig. 5 represents the output of one sensor in the x-axis with respect to the gap displacement variation for a cycle time T of 57 μs and the charging current i_s of 7.0 μA for sensor #1. Beyond the point where displacement is approximately 0.1 mm, the changing rate of the output signal slowly reduces. This is because the leakage of the electric field becomes larger as the gap displacement increases. The rotor in the collocated sensor system is separated by a gap of 0.2 mm from opposite sensors at zero point. Therefore, the output (curve 2) of another sensor in the x-axis is symmetry of the curve 1 with respect to the vertical line passing through the zero point, as seen from Fig. 5.

The plot for the differential output of opposite sensors is acquired by subtracting curve 2 from curve 1. Figs. 6 and 7 are obtained from this procedure. The experimental results of the differential signal for sensor #1 are shown in Fig. 6, and those for sensor #2 in Fig. 7. These output plots are obtained from a series of experiments in the cases of the cycle time T of 57 and 65 μs, respectively. The discharging time T_d is fixed at a value of 15 μs in all cases. The charging current i_s

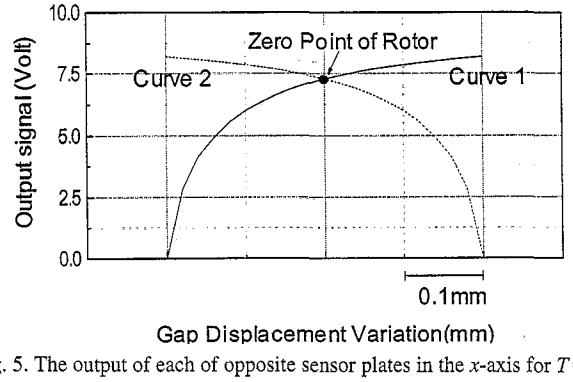

Fig. 5. The output of each of opposite sensor plates in the x-axis for $T=57$ μs and $i_s=7.0$ μA for sensor #1.

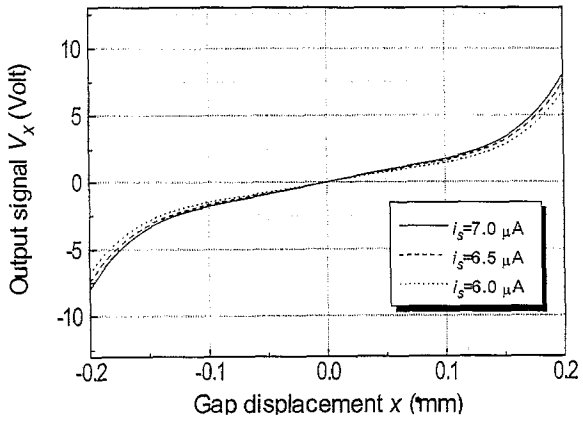

(a) Cycle time T=57μs

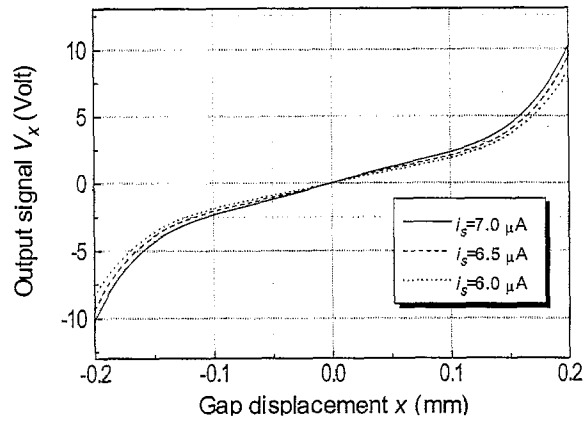

(b) Cycle time T=65μs

Fig. 6. Differential outputs of opposite sensor plates for sensor #1.

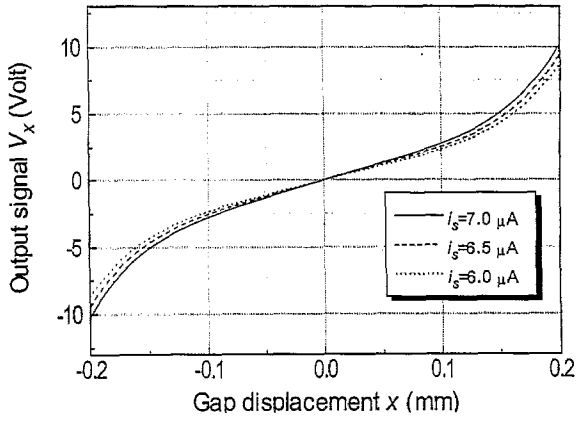

(a) Cycle time T=57μs

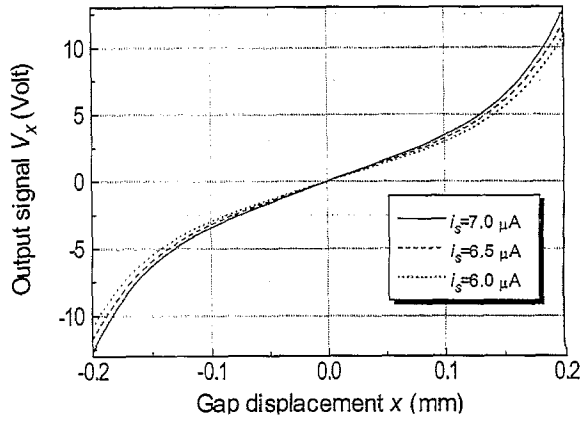

(b) Cycle time T=65μs

Fig. 7. Differential outputs of opposite sensor plates for sensor #2.

supplied to the sensor element is varied between 6.0 to 7.0 μA.

The following sensitivity characteristics are readily verified from Figs. 6 and 7.

(1) Let the output be $V_{x(1)}$ when the cycle time T_1 is 57 μs, and $V_{x(2)}$ when T_2 is 65 μs. The ratio of the rate of change of the output to the rate of change of the cycle time, $(V_{x(2)}/V_{x(1)})/(T_2/T_1)$, is 1.10 for both sensor #1 and sensor #2. The above result of the cycle time effect shows that the output increase rate is almost directly proportional to the rate of increase in cycle time.

(2) Let the output be $V_{x(1)}$ when the charging current $i_{s(1)}$ is 6.0 μA (or 6.5 μA), and $V_{x(2)}$ when $i_{s(2)}$ is 6.5 μA (or 7.0 μA). The ratio of the rate of change of the output to the rate of change of the charging current, $(V_{x(2)}/V_{x(1)})/(i_{s(2)}/i_{s(1)})$, is 1.0 for both sensor #1 and sensor #2. This result of the charging current effect shows that the rate of increase of the output is directly proportional to the rate of increase of the current.

(3) Increasing the surface area of the sensor has the effect of increasing the sensitivity [8]. The area of sensor element of sensor #2 is twice that of sensor #1. The experimental result shows that the output of sensor #2 is one and a half times that of sensor #1 if all other conditions are constant, and if the output of sensor #2 has good linearity compared to that of sensor #1.

(4) The output characteristic is nonlinear over the working range of gap displacement. The rate of increase of the output tends to remain constant up to about $x=0.125$ mm, but beyond this point the output increases, as is verified from outputs of opposite sensors in Fig. 5. For example, the sensitivity of the output with respect to the gap displacement is 26 mV/μm up to $x=0.125$ mm in case of $i_s=7.0$ μA as in Fig. 6(b), and this sensitivity is greater past point. In practice, an interpolation algorithm is used to control and correct this nonlinear characteristic.

4. Experimental evaluation on dynamic performance of the developed sensor

The bandwidth of the sensor is important in applications requiring high-speed measurements of displacement. In the control of magnetic bearings, the shaft rotates at high spinning speeds in excess of 10 000 rpm. Therefore, the bandwidth of the sensor should be high enough to enable measurements of displacement to be made quickly. A special purpose rotor, illustrated in Fig. 8, has been manufactured with an outer

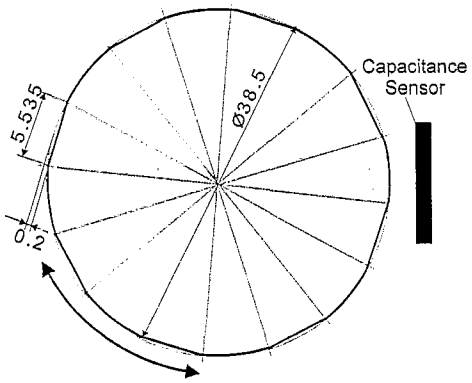

Fig. 8. Cross-section of the rotor specially designed for measuring the frequency response of the sensor (unit: mm).

diameter of 38.5 mm for measuring the bandwidth of the sensor. Eight flat segments along the perimeter of the rotor have been end-milled at equiangular intervals with a width of 5.535 mm and maximum depth-of-cut of 0.2 mm. This rotor can generate quasi-sinusoidal gap displacements that have a frequency eight times the spinning frequency of the rotor. For example, when the spinning speed of the rotor is 12 000 rpm (200 Hz), the generated quasi-sinusoidal wave will have a frequency of 1.6 kHz.

The frequency response of the sensor has been obtained from a series of experiments by changing the cycle time, the charging current and the type of sensor (whether sensor #1 or sensor #2). The experimental results show that the change in the charging current and the type of the sensor have no influence on the frequency response, provided that the cycle time is fixed to one value. That is, the frequency characteristics are not dependent on the value of the charging current and the type of the sensor, but only on the cycle time. Fig. 9 is established from this result in case of the cycle time T at 57 and 65 μs, respectively.

As the cycle time T decreases, the bandwidth of the sensor increases, as seen in Fig. 9. The bandwidth of the sensor with $T=65$ μs is about 9400 rad/s (1.5 kHz), and that of the sensor with $T=57$ μs is more than 9400 rad/s. If a higher bandwidth is desired, a lower value of the cycle time T should be selected, but the static sensitivity with respect to the gap displacement decreases, as verified from Figs. 6 and 7.

5. Application for the collocated capacitance sensor

The collocated sensor system illustrated in Fig. 1 was attached onto a test bed of a rotor system supported by magnetic bearings as shown in Fig. 10. The vertical rotor is supported by two radial magnetic bearings at both the lower and upper parts. Sensors #1 and #2 are each collocated with magnetic bearing #1 and #2. The rotor is connected to a brushless DC motor at the lower end through a flexible coupling. From the built-in encoder in the DC motor, the rotational speed of the rotor can be measured. There are two

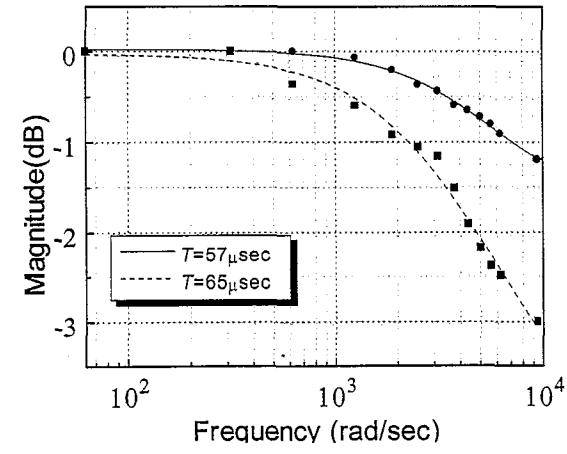

(a) Magnitude

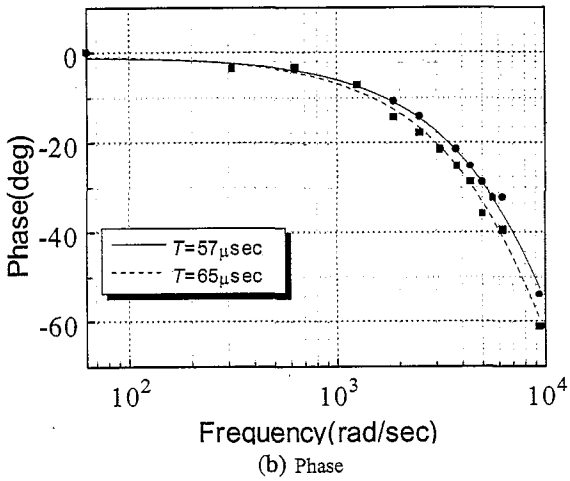

(b) Phase

Fig. 9. Frequency response of output signal for the developed sensor.

backup bearings at both ends of the shaft to protect the system in case of an emergency situation.

The feedback controller is run on a digital signal processor (DSP) with a TMS320C40 chip. The displacement signal from the sensor signal-processing unit comes to the DSP through a 12-bit analog-to-digital (A/D) converter. Through a 12-bit digital-to-analog (D/A) converter, the output signal of the DSP goes out to a pulse-width-modulation (PWM) current amplifier that generates the coil current of the magnetic bearing. The DSP board is installed into a personal computer 486 class, which can share the selected internal states with the DSP through a dual port random access memory (RAM).

Since the rigid rotor has a total of four degree-of-freedom motions in the radial direction for the upper and the lower parts, four independent feedback controllers are necessary for the regulation of the motions. The adopted feedback controller is a proportional, integral, and derivative (PID) controller, where proportional and derivative control elements stabilize the inherently unstable magnetic bearing system while the integral control element reduces a steady state regulation error. The input to the controller represents the gap displacement between the rotor and sensor. The output of the con-

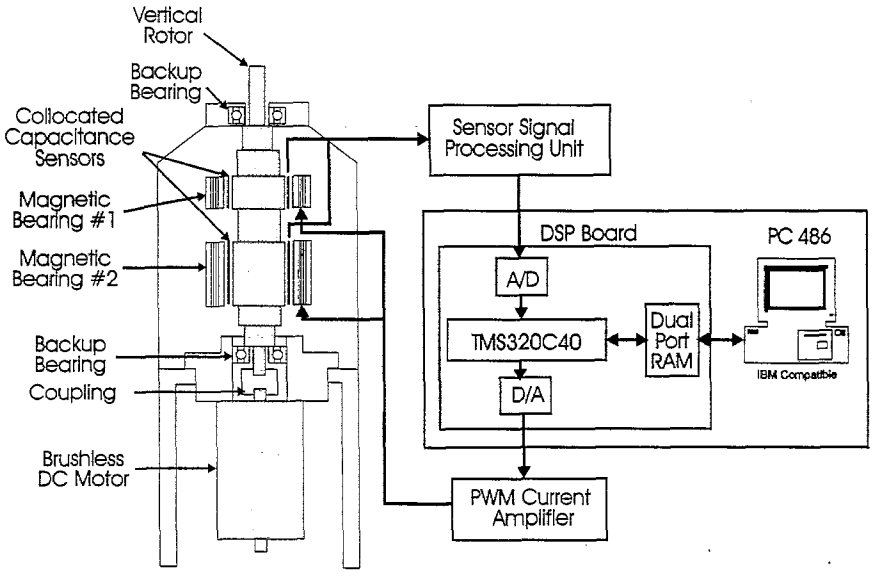

Fig. 10. Schematics for a testbed for a magnetic bearing control experiment using the collocated capacitance sensor.

troller is the command signal of the coil current of the magnetic bearing.

Let y_1, z_1 be the gap displacement for the upper part of the rotor, and y_2, z_2 the lower part. Let i_{py_1}, i_{pz_1} be the minute perturbation currents around a bias current for the upper part of the rotor, and i_{py_2}, i_{pz_2} for the lower part. Then the controller structure can be expressed as follows.

$$\frac{i_{py_1}(s)}{y_1(s)} = \frac{i_{pz_1}(s)}{z_1(s)} = K_{p_1} + K_{d_1}s + \frac{K_{i_1}}{s};$$

$$\frac{i_{py_2}(s)}{y_2(s)} = \frac{i_{pz_2}(s)}{z_2(s)} = K_{p_2} + K_{d_2}s + \frac{K_{i_2}}{s} \quad (1)$$

where K_{p_j} is a proportional gain, K_{d_j} is a derivative gain, and K_{i_j} is an integral gain.

In the experiment, the cycle time T and the charging current i_s are selected as 65 and 7.0 μA, respectively, for both sensor #1 and sensor #2. The controller gains are selected as $K_{p_1}=2200$, $K_{d_1}=1.3$, $K_{i_1}=5000$, $K_{p_2}=1300$, $K_{d_2}=0.7$, $K_{i_2}=3000$, while the bias current of the magnetic bearing coil is set to 0.5 A.

When no current flows in the magnetic bearing coil, measurements have shown that the noise level is ±0.2 μm (peak-to-peak) for both sensor #1 and sensor #2. On the control mode when the feedback controller activates the PWM current amplifier, the noise level rises to ±1.0 μm (peak-to-peak) in sensor #1 and ±0.6 μm (peak-to-peak) in sensor #2. The increase in noise level is due to the high frequency current noise of the coils generated by the PWM current amplifier. If a linear current amplifier for magnetic bearings were used, the noise level would be reduced. The resolution of the sensor is of the same order of magnitude as the noise level. Fig. 11 presents the orbit radius of the upper part of the rotor in changing the rotational speed up to approximately 10 000 rpm. At the critical speed of 2900 rpm, the orbit radius reaches the maximum value of about 20 μm. After going past the critical speed, the rotor radius approaches 11 μm, which is the same value as the mass unbalance offset of the rotor.

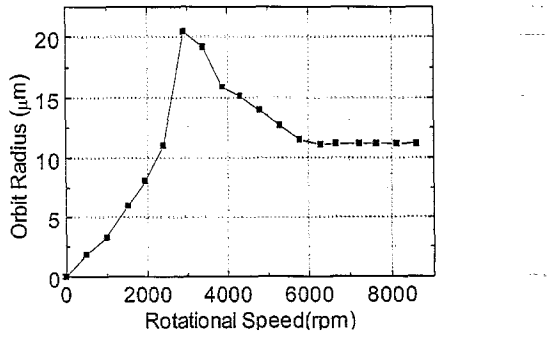

Fig. 11. Experimental result for the orbit radius of the upper part of the rotor.

6. Conclusions

A collocated sensor system has been developed with an application in magnetic bearing control. It consists of a capacitance gap sensor plate constructed by applying PCB manufacturing technology and a signal-processing unit for measuring and amplifying the charged voltages of the sensor element of the sensor plate during a cycle time.

The sensitivity of the sensor, subject to static gap displacement variations, has been measured by a series of experiments. The dynamic performance of the sensor has been measured for a variation of the cycle time. The bandwidth of the sensor was measured as 9400 rad/s when the cycle time is 65 μs, and greater when the cycle time is 57 μs. The experimental work has been carried out to verify the practicability of the collocated sensors, which are embedded into a vertical magnetic bearing supported rotor system. The noise level of the sensor increases when the PWM current amplifier generates the current required by magnetic bearing coils. It

would be expected that a linear current amplifier for the coils could reduce the noise level considerably.

This sensor system can be applied to a magnetic levitation system and other position measuring systems. Research on reducing the noise level is in progress to stabilize the performance of the sensor system. In order to achieve improved performance of the sensor, further investigations on the manufacturing technology of a more accurate sensor plate and a more elaborate alignment technique are in progress.

References

[1] M.H.W. Bonse, F. Zhu, J.W. Spronck, A new two-dimensional capacitive position transducer, Sensor and Actuators A 41–42 (1994) 29–32.

[2] P.D. Chapman, A capacitive based ultra-precision spindle error analyzer, Journal of Precision Engineering 7 (1985) 529–536.

[3] J. Boehms, R. Gerber, N.R.C. Kiley, Sensors for magnetic bearings, IEEE Transactions on Magnetics 29 (1993) 2962–2964.

[4] P.E. Allaire, R.R. Humphris, Dynamics of a flexible rotor in magnetic bearings, 4th Workshop on Rotor Dynamics Instability Problems in High Speed Turbomachinery, Texas A&M Univ., 1986.

[5] E.H. Maslen, V.S. Lefante, Transfer function zeros in noncollocated flexible rotor models, 3rd International Symposium on Magnetic Bearings, Alexandria, VA, USA, 1992, pp. 242–252.

[6] L.E. Barrett, T.S. Brockett, E.H. Maslen, Analysis of rotors with noncollocated magnetic bearings using transfer matrices, Proc. of MAG'92, 1992, pp. 144–154.

[7] A.O. Salazar, W. Dunford, R. Stephan, E. Watanabe, A magnetic bearing systems using capacitive sensor for position measurement, IEEE Transactions on Magnetics 26 (1990) 2541–2543.

[8] M.A. Brown, C.E. Bullied, The effect of tilt and surface damage on practical capacitance displacement transducers, J. Phys. E. Sci. Instr. 11 (1978) 429–432.